Breaking hydrogen bond in metal free carbon nitride to induce peroxymonosulfate nonradical activation: Surface-mediated electron transfer

Jingjing Jiang [a,b], Chenli Yue [a,b], Ziqing Zhao [a,b], Di Wu [c,d], Shengda Liu [e], Yanan Zhang [a,b], Bowen Zhao [a,b], Zhenhao Zhao [a,b], Yansong Liu [a,b], Cong Lyu [a,b], Chongjun Zhang [f], Mingxin Huo [f], Dandan Zhou [f], Shuangshi Dong [a,b,*]

[a] *Key Laboratory of Groundwater Resources and Environment (Jilin University), Ministry of Education, Jilin University, Changchun, Jilin 130021, China*
[b] *Jilin Provincial Key Laboratory of Water Resources and Environment, Jilin University, Changchun, Jilin 130021, China*
[c] *Centre for Environment and Energy Research, Ghent University Global Campus, Incheon, South Korea*
[d] *Department of Green Chemistry and Technology, Ghent University, and Centre for Advanced Process Technology for Urban Resource Recovery, Ghent, Belgium*
[e] *School of Chemical and Environmental Engineering, Changchun University of Science and Technology, Changchun, Jilin 130022, China*
[f] *Engineering Lab for Water Pollution Control and Resources Recovery of Jilin Province, School of Environment, Northeast Normal University, Changchun, Jilin 130117, China*

ARTICLE INFO

ABSTRACT

Breaking hydrogen bond in metal free carbon nitride (CN) to increase peroxymonosulfate (PMS) adsorption for surface-mediated electron transfer has been challenging. Herein, we incorporated N−C≡N monomer into CN to break hydrogen bond by the introduction of polyvinylpyrrolidone (PVP). The developed nonradical oxidation system achieved selective decomposition of highly hydrophilic contaminants and efficient removal of chemical oxygen demand (58.0%), total phosphorus (88.1%), ammonia nitrogen (100.0%) and total nitrogen (67.8%) from the secondary effluent in a continuous flow reactor. This was attributed to that the breakage of hydrogen bond accelerated the redistribution of electron densities at C and N sites, leading to an increase in the adsorption energy of N site to PMS. This promoted the formation of PVP/CN-PMS* complex for the selective and efficient removal of organics and inorganics. This work provided a new perspective for the selective and long-term treatment of practical wastewater.

1. Introduction

The metal-free materials have been widely used in wastewater treatment because they can prevent secondary pollution caused by toxic metal ions. [1,2]. The metal-free CN-induced PMS-based photo--Fenton-like technology had gained widespread attention in PMS activation due to its ability to enhance PMS adsorption [3] and to extend the O−O bond of PMS [4]. This was achieved by the involvement of N atom, which acted as a Lewis acid site [5], as well as the participation of photogenerated electrons [6]. There were two main types of PMS activation: radical and nonradical [7]. Nonradical activation, in particular, has shown resistance to water matrix interference and remarkable advantage in selective treatment of complex wastewater [8,9].

However, the nonradical activation of PMS has been accompanied by radical activation with the generation of strongly oxidizing $SO_4^{\bullet-}$ and •OH, leading to the susceptibility of photo-Fenton-like system to be a radical-dominated oxidation system [10]. It was urgent to develop method for the targeted construction of PMS-based nonradical oxidation system.

The surface-mediated electron transfer has been recognized as one of the effective PMS-based nonradical reaction [11]. It has been demonstrated that an increased ratio of surface-mediated electron transfer pathway leaded to higher degradation efficiency of contaminants [12]. Previous research has reported a strong correlation between PMS adsorption and surface-mediated electron transfer [13] and the PMS adsorption was related to the electron densities of C and N atoms [14,

15]. Therefore, we anticipated that enhancing the adsorption energy of CN on PMS would contribute to developing a PMS-based photo-Fenton-like system that was dominated by the surface-mediated electron transfer. However, the presence of hydrogen bond in CN posed a challenge in redistributing the electron densities of C and N atoms due to the localization of electrons in the melon [16,17], thereby hindering the enhancement of PMS adsorption energy [18,19].

The introduction of N−X bond into the polymeric melon units of CN had the potential to break the hydrogen bond [20]. Previous research has shown that polyvinylpyrrolidone (PVP) could introduce carbon-containing functional groups that distributed hydrogen bond [21,22]. Based on these inspirations, we hypothesized that incorporating PVP in the preparation of CN could break hydrogen bond and increase the adsorption energy of PMS by introducing carbon-containing functional groups. This would facilitate the formation of PVP/CN-PMS* complex and create a surface-mediated electron transfer system. Currently, although there have been researches on the construction of surface-mediated electron transfer system based on CN, to the best of my knowledge, there has been no precedent for enhancing surface electron transfer by increasing the adsorption energy in a hydrogen-bond engineering perspective.

Herein, we proposed to reduce the hydrogen bond of CN by introducing PVP during the preparation process of CN with the aim of (i) constructing a photo-Fenton-like system that was primarily driven by electron transfer; (ii) analyzing the change in the hydrogen bond of CN based on the results of X-ray diffraction (XRD) spectra, electron paramagnetic resonance (EPR) spectra and x-ray photoelectron spectroscopy (XPS); (iii) investigating the effect of hydrogen bond on electron density, adsorption energy and PMS activation pathway according to theoretical and experimental results; (iv) revealing the relationship of hydrogen bond and surface-mediated electron transfer; (v) elucidating the selective removal of representative contaminants in various fields by surface-mediated electron transfer system and (vi) exploring the stability of the developed nonradical oxidation system to validate its practical application.

2. Materials and methods

2.1. Chemicals and characterizations

All chemicals were of analytical grade and have not been further purified. Urea, polyvinylpyrrolidone, sodium thiosulfate, isopropanol, β-carotene, methanol, 2,2,6,6-tetramethyl-1-piperidinyloxy, sodium oxalate, potassium bromate, sodium chloride, bicarbonates, sodium nitrate and sodium phosphate were purchased from Aladdin Biological Technology Co., Ltd. Methanol and acetonitrile were purchased by Anpel Laboratory Technologies Co., Ltd. The emergency antibiotic wastewater composed of 0.04 mM tetracycline hydrochloride, 1.64 mM sodium chloride, 11.5 mM bicarbonates, 0.7 mM sodium nitrate, 0.016 mM sodium phosphate and 10.0 mg/L dissolved organic matter was prepared.

Transmission electron microscopy (TEM), high-resolution transmission electron microscopy (HRTEM) images and scanning TEM (STEM)-EDX elemental mapping were analyzed by a JEOL JEM-2010 microscope (accelerating voltage = 200 kV). XRD pattern were recorded by a Rigaku D/Max-2550 diffractometer via Cu Kα radiation at 50 kV and 200 mA. Fourier transform infrared (FT-IR) spectra were obtained using a VERTEX 70 spectrophotometer (Bruker, Germany). The XPS measurements were performed by a Thermo VG Scientific ESCALAB 250 spectrometer. UV–vis diffuse reflectance spectra (DRS) were obtained by a UV–vis-NIR spectrophotometer (Shimadzu UV-3600). The EPR measurements were performed on a Brooke 300 system. The total organic carbon (TOC) removal efficiencies of different samples were detected by a TOC analyzer (SSM-5000A). Electron spin resonance (ESR) spectra of reactive oxidation species trapped in water and methanol by DMPO or TEMP were obtained by a Brooke A300 system. Room temperature steady photoluminescence (PL) was identified by a FLUOROMAX-4. The TCH degradation products were analyzed with liquid chromatograph mass spectrometer (HPLC-MS) system (Details in Text S1). The photoelectrochemical performance was measured on a CHI 660E electrochemical workstation (Details in Text S1).

2.2. Synthesis of PVP/CN

1.35 g CN prepared according to previous work [23] and certain mass of PVP (mass ratio of PVP to CN at 0.005%, 0.01%, 0.03% and 0.05%) was dispersed into 50.0 mL ethylene glycol. After stirring for 24 h, the above mixture was dried at 60 ℃ for 12 h and then calcined at 400 ℃ for 3 h. The resulting samples were named as xPVP/CN (x = 0.5, 1, 3 and 5).

2.3. Catalytic performance evaluation

In the static experiment, 0.01 g sample was added into 20 mL tetracycline hydrochloride (TCH, 0.04 mM), 4-chlorophenol (4-CP, 0.04 mM), bisphenol A (BPA, 0.04 mM), atrazine (ATZ, 0.04 mM), sulfamethoxazole (SMX, 0.04 mM) and carbamazepine (CBZ, 0.04 mM) aqueous solution, respectively. The reaction was activated after the introduction of PMS and visible light. The visible light was generated by a 300.0 W xenon lamp (CEL-HXF 300, Beijing Education Au-light Co., Ltd.) equipped with a cut-off filter (<420 nm). The light intensity was measured at 131.2 mW/cm^2, with a irradiation area of 3.34 cm^2. During the reaction, a 2.0 mL sample was collected every 10 min and filtered through a 0.22 μm membrane prior to the addition of excess sodium thiosulfate (1.0 mM $Na_2S_2O_3$). The initial pH was modulated by manually adding HCl and NaOH as needed (less than 0.2 pH unit change). In active species scavenger experiment, isopropanol, β-carotene, methanol, 2,2,6,6-tetramethyl-1-piperidinyloxy, sodium oxalate and potassium bromate were selected as •OH, $^1O_2$, •SO_4^- •O_2^-, h$^+$ and e$^-$, respectively.

The continuous flow experiments were performed in a reactor with the column diameter of 4.5 cm and the column height of 35.0 cm (Fig. S1). The four 3PVP/CN-fiber balls (approximately 3.5 cm in diameter) were added to the column to ensure that 0.5 g catalyst remained in the reactor per liter, and then two blank fiber balls were added to the top of 3PVP/CN-fiber balls to avoid 3PVP/CN detachment during continuous flow. The detailed preparation of 3PVP/CN-fiber balls was described in Text S2. Tap water with TCH was selected as the configured emergency antibiotic wastewater. The secondary effluent from the Jilin petrochemical company wastewater treatment plant was used as the practical wastewater. The photo-Fenton-like reaction was activated when TCH and PMS passed through the 3PVP/CN-fiber balls in the continuous flow reactor at a flow rate of 50 mL/min and hydraulic retention time of 11.2 min under visible light irradiation. The light intensity was measured at 131.2 mW/cm^2, with a irradiation area of 3.34 cm^2. The samples were taken at intervals within 30 days to determine the concentration of contaminants in wastewater.

2.4. Analytical methods

The concentration of various contaminants in different fields was detected using high-performance liquid chromatography (HPLC) (Details in Table S1). The concentration of PMS was obtained using a DRS at 352 nm (Details in Text S3). The density functional theory (DFT) calculation was performed using the Gaussian 16 package (Details in Text S4). The toxicity of TCH and its products was estimated using the toxicity estimation software tool (T.E.S.T.) in the consensus method. The cytotoxicity assays were conducted to investigate the growth inhibition of luminescent bacteria (Details in Text S5).

3. Results and discussion

3.1. Characterizations of catalysts

The TEM images (Fig. S2) showed that CN and 3PVP/CN had similar ultrathin nanosheets. This indicated that the introduction of PVP has not changed the morphology. Breaking the hydrogen bonds of CN would contribute to the formation of extended π-conjugated system for enhanced crystallinity of CN [24,25]. The crystallinity of 3PVP/CN was higher than that of CN, which was supported by the clear lattice spacing of 0.32 nm for (002) plane of 3PVP/CN than CN in HRTEM, Fig. 1a) [26] and enhanced crystallinity value from 0.64 to 0.68 in XRD spectra (Table S2, Fig. 1b). In FT-IR spectra (Fig. 1c), the peak of $-NH_2/=NH$ groups shifted from 3414 to 3270 cm^{-1} after the introduction of PVP into CN (Fig. 1c). This was attributed to the uneven distribution of the electron cloud density by the breakage of hydrogen bond for the increase in vibrational frequency [27]. For CN, both the proton of amine and the proton attached to the hybridized sp^3 N enable the formation of hydrogen bond. The higher the ratio of sp^2 N−C=N, the lower amount of proton. As the mass ratio increased from 0% to 5%, the ratio of sp^2 N−C=N increased from 0.16 to 0.63 (Table S3 and S4) in XPS (Figs. 1d and 1e), in well consistence with the increased C ratio from 31.21% to 31.68% in element analysis (Fig. S3). This result was similar to that in previous work [28]. Compared to CN, the EPR signal with the g value of 2.003 by 3PVP/CN was enhanced, demonstrating that the breakage of hydrogen bond redistributed the electron [29] (Fig. 1 f). The above results evidenced that the amount of hydrogen bond in PVP/CN was less than that in CN. The CN and PVP/CN models were schematically shown in Fig. S4. Combined with the negligible change in D and G band intensity of PVP/CN with different mass ratio of PVP compared to those of pristine CN in Raman spectra (Fig. S5) and no carbon quantum dots in TEM image (Fig. S2), it was further confirmed that the introduction of PVP mainly broke hydrogen bond rather than producing carbon quantum dots.

3.2. Decontamination performance by surface-mediated electron transfer

Fig. 2a exhibited that neither visible light nor PMS alone effectively degraded TCH. However, CN removed 72.4% of TCH, with removal efficiency firstly increasing and then decreasing as the mass ratio of PVP increasing from 0% to 0.05% in PMS/vis system. In the PMS/vis system with the catalyst dosage of 0.2 g/L and the TCH concentration of 0.04 mM, 3PVP/CN achieved an optimal TCH removal efficiency (90.0%) in 60 min (Fig. S6), higher than those of the PMS-based Fenton-like system (55.9%) and the photocatalytic system (46.3%) (Fig. S7). The difference in TCH removal efficiency between the PMS/vis system and the other two systems, using 3PVP/CN, was greater than that between the PMS/vis system and the other two systems using CN. This difference could be attributed to the fact that PVP broadened the light absorption range (Fig. S8) and enhanced the separation and transfer of photogenerated charges (Fig. S9). The correlation plot of degradation rate constant k_{obs} and normalized k based on the surface area (k_{BET}) with various possible influencing factors demonstrated that the crystallinity was related to k_{BET} (p $<$ = 0.05) (Fig. 2b and S10, Text S6). Given that the crystallinity was related to the amount of hydrogen bond [30,31] and only 1.2% higher removal efficiency by 3PVP/CN without calcination (73.6%) than that by CN in PMS/vis system (Fig. S11), it was confirmed that the hydrogen bond in CN mainly affected TCH removal in 3PVP/CN/PMS/vis system.

In Fig. 2c, the contribution ratio of electron transfer pathway in 3PVP/CN/PMS system was 73.5%, which was much higher than those of •OH (7.4%), $^1O_2$ (15.4%) and $SO_4^{\bullet-}$ (3.7%), respectively. However, a completely different result was found in CN/PMS system. The •OH contributed 51.1% of TCH removal in CN/PMS system, which was much
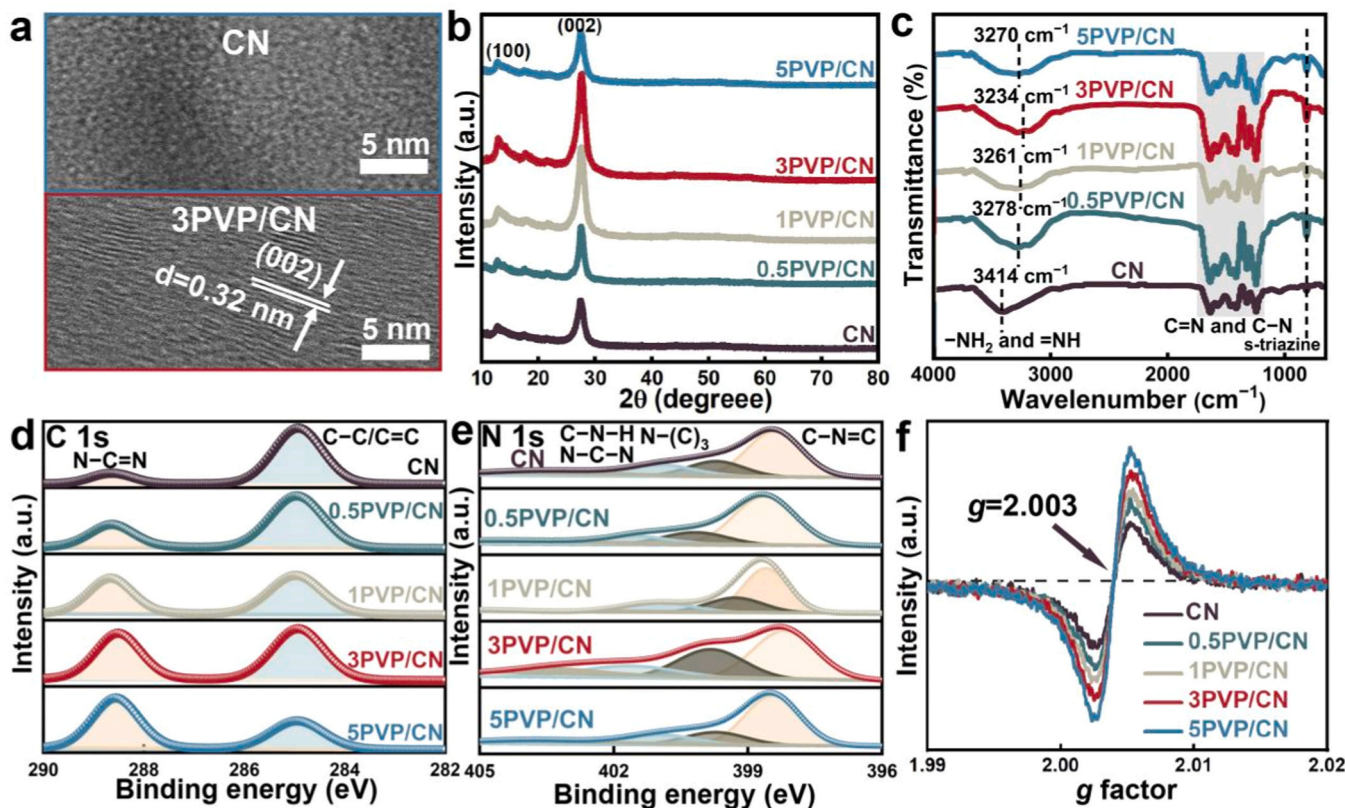

Fig. 1. (a) HRTEM images of CN and 3PVP/CN; (b) XRD pattern, (c) FT-IR spectra, (d) C 1 s spectra, (e) N 1 s spectra and (f) EPR spectra of as-prepared catalysts, respectively.
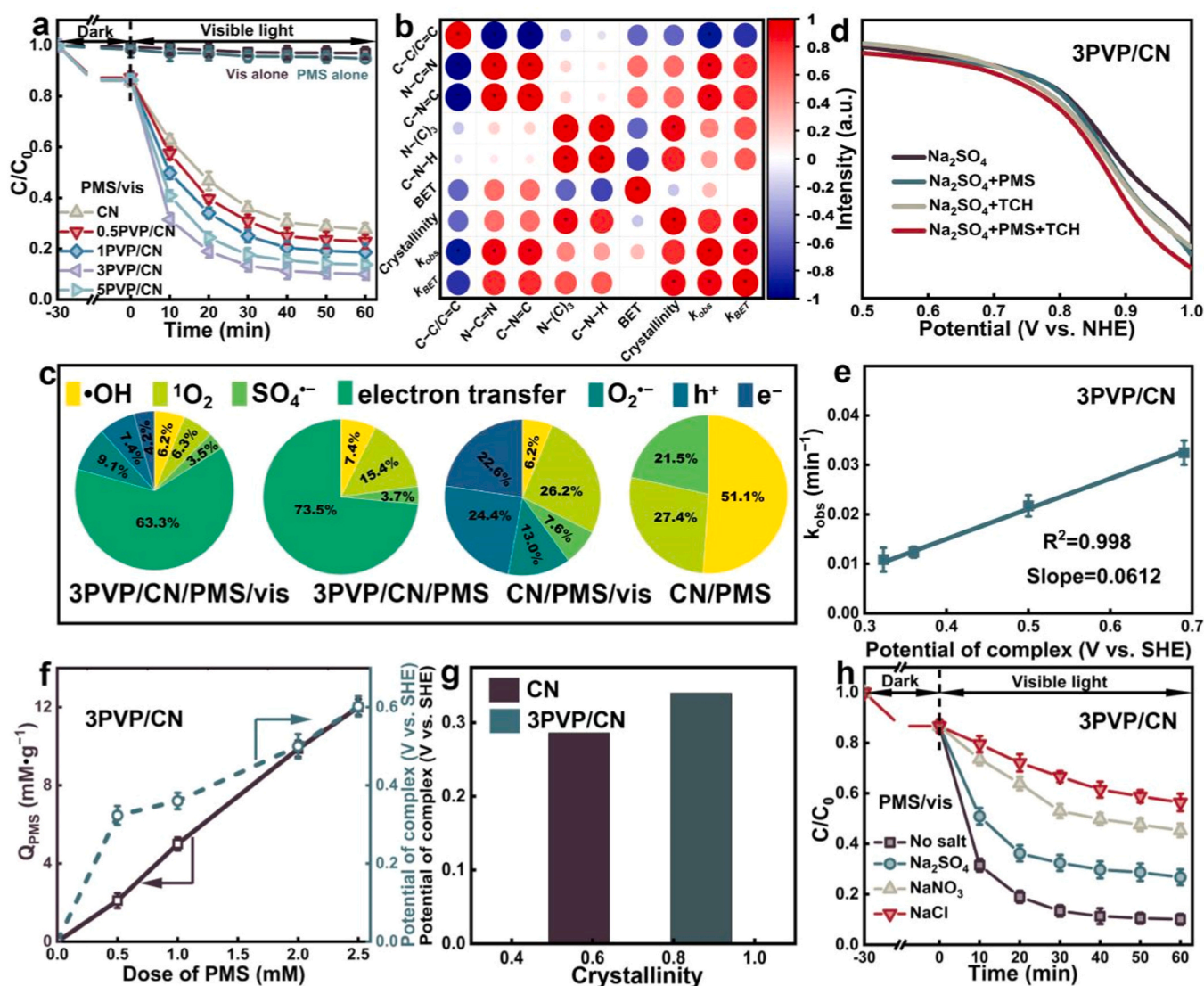
Fig. 2. (a) Removal of TCH by as-prepared catalyst; (b) Contribution of different factors on removal of TCH in PMS/vis system, *represents $P <= 0.05$; (c) Active species contribution in TCH removal by CN and 3PVP/CN under different systems; (d) LSV curves of 3PVP/CN under different conditions; (e) correlation between k_{obs} and potential of complexes; (f) correlations of PMS adsorption quantity and potential of complexes with the dose of PMS; (g) Correlation between potential of complexes and the crystallinity of CN; (h) Removal of TCH by 3PVP/CN in the presence of inorganics in PMS/vis system.

higher than other active species. The above results demonstrated that breaking the hydrogen bond of CN transformed the system from •OH-mediated oxidation into surface-mediated electron transfer. The introduction of visible light resulted in a change in the major reactive species in the CN/PMS/vis system from $O_2^{•-}$ to $^1O_2$. This change occurred as H^+ further reacted with $O_2^{•-}$ to form $^1O_2$ [32]. Despite the introduction of secondary reaction by visible light, the dominant electron transfer pathway remained between 3PVP/CN and PMS due to their close interaction. The detailed analysis of various active species generation was exhibited in Text S7. The linear cyclic voltammetry (LSV) signals of PMS and TCH combined showed higher values compared to PMS or TCH alone. This observation suggested the existence of mediated electron transfer pathways in the 3PVP/CN/PMS/vis system [33,34]. In contrast to the decreased LSV signal observed when TCH was introduced into the CN/PMS system (Fig. S14). In the 3PVP/CN/PMS/vis system, the open-circuit voltage sequentially increased with the addition of PMS and TCH (Fig. S15). This result provided additional evidence supporting the existence of the mediated electron transfer pathway.

To further confirm the role of electron transfer pathway in 3PVP/CN/PMS/vis system, we correlated the k_{obs} with potential of complex

(Fig. 2e). A linear relationship between the k_{obs} and the potential of complex based on the first-order kinetic model: $k_{obs} = 0.0612 \times \text{potential}_{complex} - 0.0095$ ($R^2 = 0.998$) (Eq. 1). This meant that the degradation kinetics of TCH was positively related to the potential of 3PVP/CN-PMS* complex. Fig. 2 f and S16 exhibited that the PMS adsorption capacity and the potential of 3PVP/CN-PMS* complex enhanced with increasing PMS amount from 0.0 mM to 2.5 mM. The breakage of hydrogen bond enabled electron delocalization of melon and redistribution of electron density in CN [35,36], which was positively correlated with PMS adsorption [37]. Therefore, the higher dosage of PMS, the higher adsorption capacity and the higher potential of 3PVP/CN-PMS* complex. Fig. 2 g and S17 exhibited that the crystallinity of CN was positively associated with the potential of 3PVP/CN-PMS* complex and k_{BET}. It was demonstrated that 3PVP/CN enhanced the adsorption of PMS, resulting in an increased potential of the catalyst-PMS complex for TCH removal. That is, the hydrogen bond affected the potential of 3PVP/CN-PMS* complex. The addition of sodium sulfate (Na_2SO_4), $NaNO_3$ and NaCl inhibited the TCH removal by 16.7%, 35.3% and 46.4% in 3PVP/CN/PMS/vis system, respectively. Compared to the degradation efficiency of TCH in deionized water, the

3PVP/CN system exhibited a reduction in TCH degradation efficiencies of 1.6% and 2.4% in tap water and secondary effluent, respectively (Fig. S18). The main reason for this was that the adsorption sites of PMS were occupied by inorganic ions. The TCH removal efficiencies by CN in tap water and secondary effluent were much lower compared to its removal in deionized water. This could be primarily attributed to the reaction between $SO_4^{•-}$, •OH, and other radicals with inorganic ions in the water matrix, resulting in the formation of weakly oxidative radicals.

Based on the result of high performance liquid chromatography-mass spectrometry (HPLC-MS, Fig. S19), the possible TCH degradation pathway in surface-mediated electron transfer system was proposed (Fig. S20). The TCH with the m/z of 445 was transformed into P1 (m/z=429), P2 (m/z=410), P3 (m/z=417), P4 (m/z=369), P5 (m/z=337), P6 (m/z=359), P7 (m/z=327) and P9 (m/z=343) via dehydroxylation [38,39], demethylation [40] and deamination reactions [41,42]. The C−C bonds of P5 and P9 were then cleaved into three-ringed P8 (m/z=269) [43], P10 (m/z=241) [44], P11 (m/z=278) [45] and P12 (m/z=252) [46]. The P10 (m/z=241) was demethylated to P12 (m/z=225) [47], which was further transformed into P14 by cleaving the C−C bond. Eventually, all intermediates were transformed into CO_2 and H_2O.

3.3. The surface-mediated electron transfer mechanism

In *in-situ* Raman spectra (Fig. 3a), the peaks at 1060, 979, and 882 cm^{-1} corresponded to HSO_5^-, SO_4^{2-} and O−O of PMS, respectively [48]. The coexistence of 3PVP/CN and PMS was followed by the appearance of a new signal at 838 nm, corresponding to the formation of the PVP/CN-PMS* complex [49]. In contrast, this signal was not observed when CN and PMS coexisted. In the PMS/vis system, the 3PVP/CN exhibited a PMS removal efficiency of 66.7%, which was 60.9% higher than that of CN (Fig. 3b). The PMS removal efficiency decreased slightly to 62.2% and 64.1% by 3PVP/CN after the introduction of $Na_2C_2O_4$ (a h^+ scavenger) and Cr^{6+} (an e^- scavenger), respectively, indicating that 7.1% of PMS was activated and 59.6% of PMS was adsorbed. The PMS removal efficiency decreased from 5.9% to 2.8% and to 4.7% by CN after the addition of $Na_2C_2O_4$ and Cr^{6+}, respectively, illustrating that 4.3% of PMS was activated and only 1.6% of PMS was adsorbed for electron-transfer (Fig. S21). With the addition of TCH, the PMS removal efficiency of 3PVP/CN was enhanced by 5.4%, as illustrated in Fig. 3c. However, the PMS removal efficiency hardly changed with the addition of TCH. These results evidenced that 3PVP/CN, but not CN, could form a complex with PMS to efficiently extract electrons from TCH. Fig. 3e illustrated that the adsorption energy between PMS and the N site of 3PVP/CN was −4.34 eV, which was much lower than that of the C site (−4.26 eV). Interestingly, the adsorption
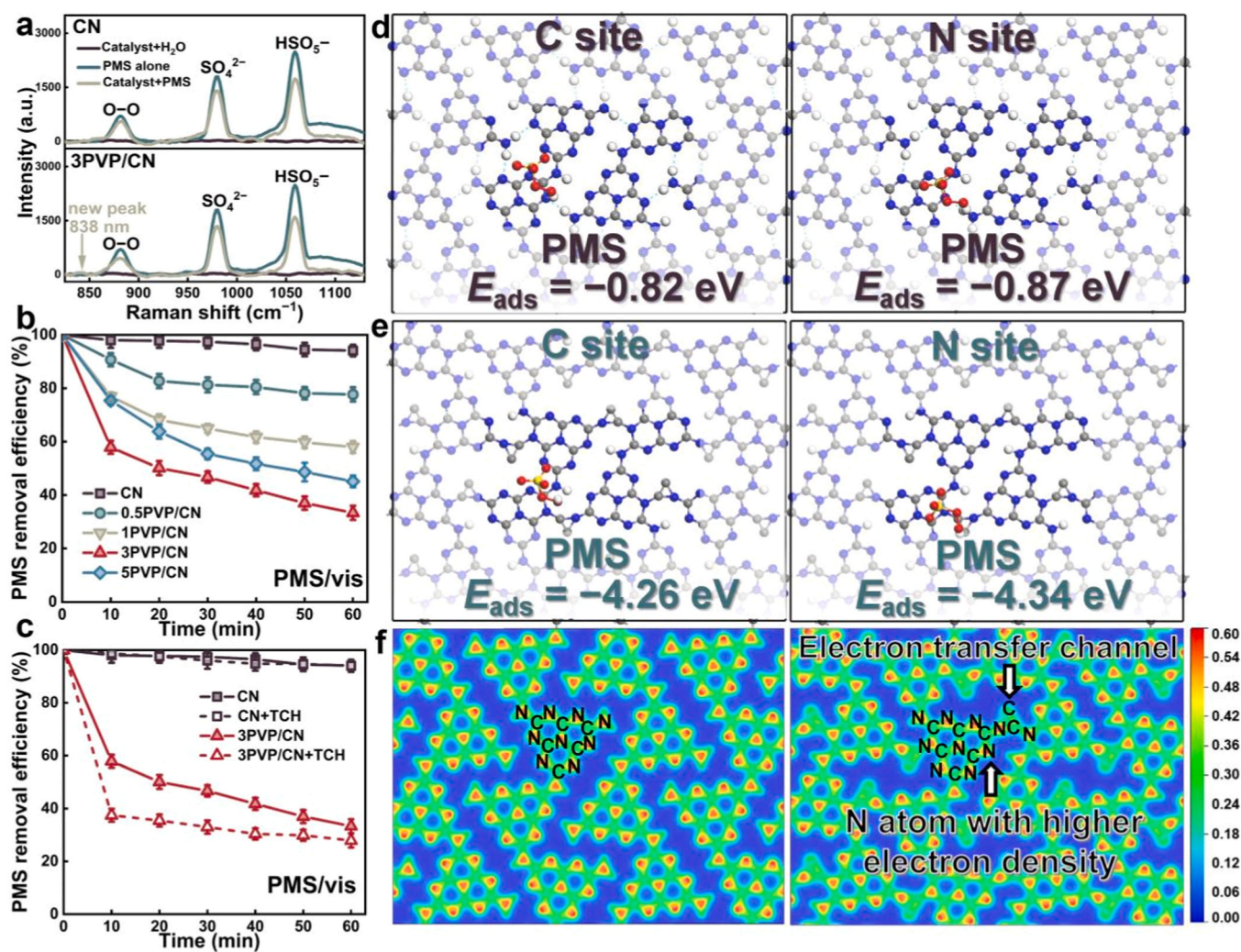

Fig. 3. (a) The *in-situ* Raman spectra of CN and 3PVP/CN under different conditions; (b) PMS concentration of catalysts in the PMS/vis system; (c) PMS removal of CN and 3PVP/CN within/out TCH; PMS adsorption on (d) CN and (e) 3PVP/CN with C and N sites, respectively; (f) Two-dimensional valence-electron density color-filled maps of CN (left) and 3PVP/CN (right), respectively.

energy between PMS and N site of 3PVP/CN was even more negative compared to CN (−0.87 eV) (Fig. 3e). The color-filled maps of two-dimensional valence-electron density (Fig. 3 f) showed that the electron density at the N site of 3PVP/CN was higher than that of CN. These findings indicated that the breakage of hydrogen bond influenced the electron density, promoting the adsorption of PMS at the N site and facilitating the formation of intermediate complex.

We evaluated the reactivity of surface-mediated electron transfer pathway towards various representative contaminants. The 27.6% of 4-CP, 43.8% of BPA, 15.0% of ATZ, 96.4% of SMX and 16.2% of CBZ were removed in 3PVP/CN/PMS/vis system. To understand the selective removal of surface-mediated electron transfer system, different molecular descriptors such as n-octanol/water partition constant (Kow), energy gap (E_{PD}), ionization potential (IP), Hammett substituent constant (σ^+) and dissociation constant (pKa) were correlated with removal efficiency (Fig. S22). Based on the first-order kinetic model: Removal efficiency(%) $= -43.5307 \times \log k_{OW} + 132.4204$ (Eq. 2), a strong linear relationship ($R^2 = 0.991$) was observed between the removal efficiency of contaminants and logKow. This finding demonstrated that the surface-mediated electron transfer pathway was effective in removing hydrophilic contaminants (Fig. 4b). However, the relationship constant between removal efficiency and various molecular descriptors was consistently below 0.614 (Fig. S23). This finding provided further evidence for the coordinated effect of multiple active species in the CN/PMS/vis system. To rule out the possibility that PVP led to the selective removal of hydrophilic contaminants by changing the hydrophilicity of CN instead of inducing electron transfer pathways, we measured the contact angles of the catalysts. Fig. S24 exhibited that the variations contact angles did not coincide with the trend of the removal of representative contaminant, TCH, suggesting that the effect of PVP on the hydrophilicity of CN was not a major factor.

Based on the aforementioned findings, we could conclude that the N−C≡N monomer, formed as a result of the reduction of the hydrogen bond in CN by PVP, served as an electron transfer motor. This motor delocalized electrons in the melon to redistribute the electron density of CN and enhanced the adsorption energy of N site to PMS, thus increasing the oxidation potential of the PVP/CN-PMS* complex for the accelerated removal of hydrophilic contaminants (Fig. 4c).

3.4. Practical application potential

To evaluate the potential for practical application of 3PVP/CN, the continuous flow reactor containing 3PVP/CN was employed for the removal of contaminants during 30 days running. The schematic diagram of the device and experimental equipment was presented in Figs. 5a and 5b, respectively. The TCH removal efficiencies by the blank fiber balls with/without PMS was both ~8.0%, respectively (Fig. S25). The result demonstrated that the blank fiber ball could adsorb partial TCH but was almost unreacted with PMS. After subtracting the TCH removal in PMS/vis system by blank fiber ball, 90.6% of TCH was removed by 3PVP/CN from the laboratory-configured emergency antibiotic wastewater during the 30-day continuous run. Although the removal efficiency of CN also exceeded 67.3%, its degradation efficiency exhibited greater fluctuations compared to 3PVP/CN. The TOC removal efficiency of 3PVP/CN reached a 21.1% higher efficiency compared to CN. To further evaluate the removal performance of the 3PVP/CN/PMS/vis system, we chose the secondary effluent from the Jilin petrochemical company wastewater treatment plant. Fig. S26 showed that the chemical oxygen demand (COD), total phosphorus (TP), ammonia nitrogen (NH_4^+-N) and total nitrogen (TN) removal efficiencies of secondary effluent by the blank fiber balls in PMS/vis system were 3.15%, 1.24%, 6.49% and 6.29%, respectively. After subtracting the effect of blank fiber balls, the removal efficiencies of COD and TP by 3PVP/CN could reach 58.0% of COD and 88.1% of TP at 60 min. The COD and TP remained stable between 60 min and 30 day. Removal efficiency of NH_4^+-N was 100% at 90 min and then stabilized at 100% due to the conversion of NH_4^+-N to nitrogen gas by surface-mediated electron transfer pathway. The TN removal was achieved in 67.8% at 30 min, with almost no obvious change in removal efficiency after 30-min. The almost unchanged physical phase and functional group structure of 3PVP/CN before and after reaction evidenced the excellent stability of the surface-mediated electron transfer system (Fig. S27).
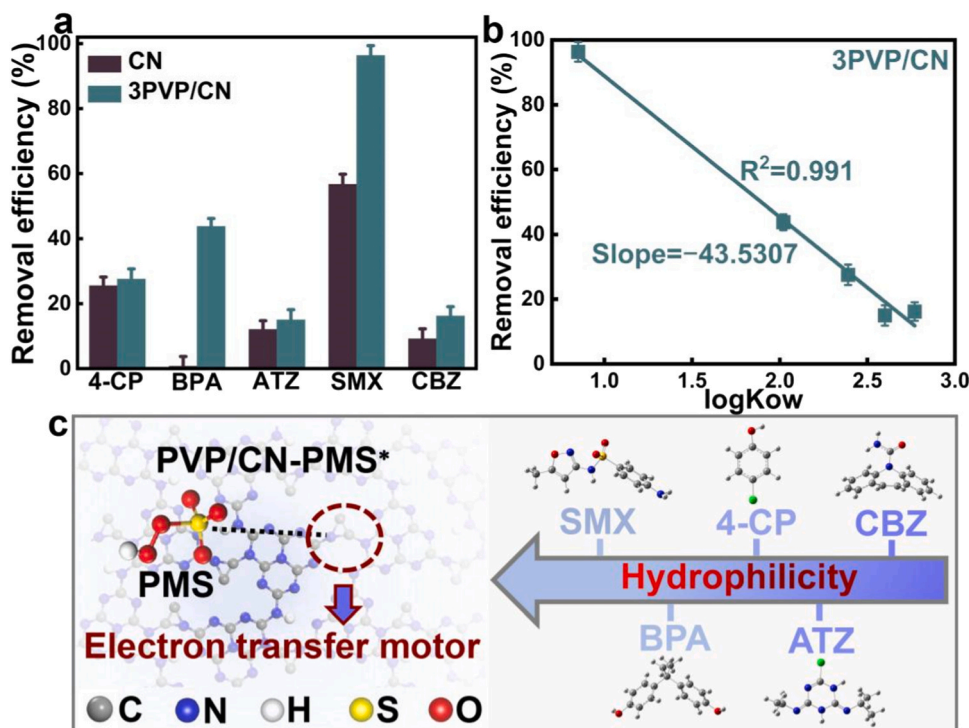

Fig. 4. (a) Removal efficiencies of various contaminants by CN and 3PVP/CN; (b) Correlation between removal efficiencies of various contaminants with logKow in 3PVP/CN/PMS/vis system; (c) Schematic diagram of selective contaminant removal by PVP/CN.
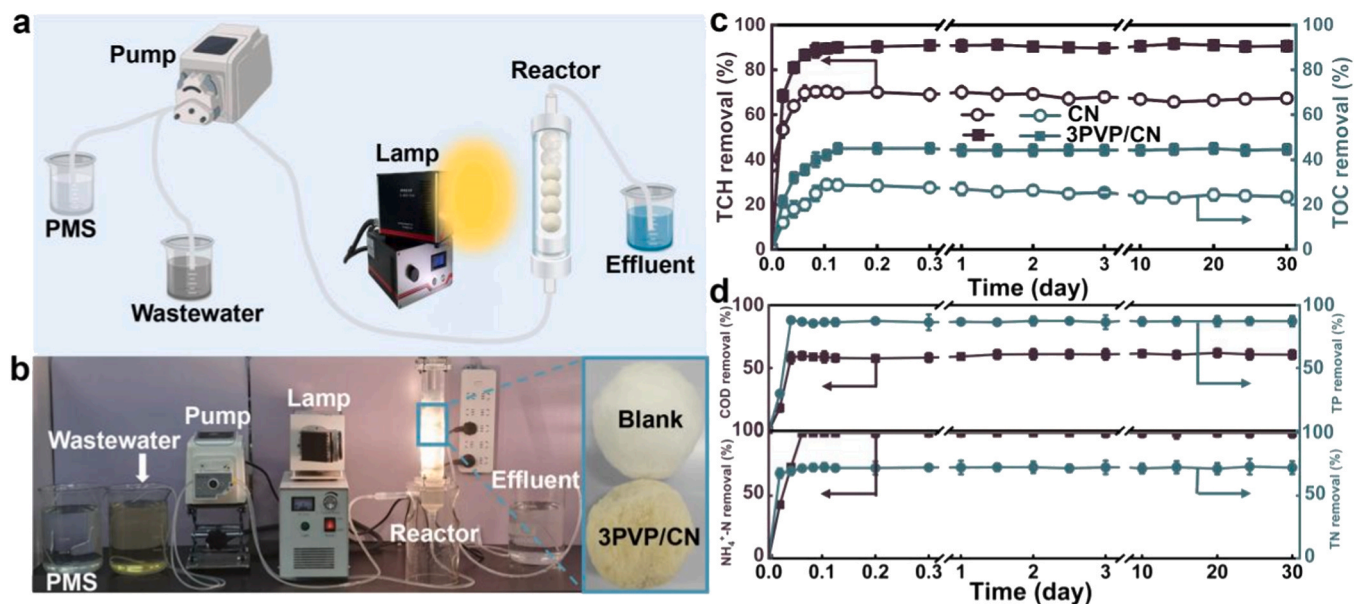
Fig. 5. (a) Schematic illustration of small-scale wastewater treatment process; (b) Photograph of wastewater treatment experiment equipment; (c) TCH and TOC removal efficiencies of configured emergency antibiotic wastewater by CN and 3PVP/CN, respectively; (d) COD, TP, NH_4^+-N and TN removal of secondary effluent in 3PVP/CN/PMS/vis system. $[COD]_0$=58.44 mg/L; $[TP]_0$=16.58 mg/L; $[NH_4^+$-N$]_0$=25.63 mg/L; $[TN]_0$=47.90 mg/L.

To assess the toxicity of the products, luminescent *vibrio cyanobacteria* were employed in growth inhibition assays (Fig. S28). The specific details could be found in Text S8. The inhibition ratios of *vibrio cyanobacteria* by $^1O_2$ and $\bullet SO_4^-$-mediated systems were higher than that of TCH after 20 min but lower after 40 min. The inhibition ratios of *vibrio cyanobacteria* by $^1O_2$ and $\bullet SO_4^-$-mediated systems were even lower than TCH after 60 min. The inhibition ratio of *vibrio cyanobacteria* in the $^1O_2$-mediated system after 60 min decreased to 14.6%, which was lower than the inhibition ratio of 23.8% in the $\bullet SO_4^-$-mediated system. The values of acute toxicity, developmental toxicity and mutagenicity for most products were found to be lower compared to TCH (Fig. S29). These experimental and theoretical results provided evidences that the surface-mediated electron transfer pathway was effective in degrading toxic TCH into less-toxic products.

4. In conclusion

This study overcame the limitation of the tendency to develop photo-Fenton technology dominated by radical rather than nonradical by breaking hydrogen bond in CN. The breakage of hydrogen bond redistributed the electron densities of C and N sites, leading to an increase in the adsorption energy of N site to PMS. This accelerated the formation of PVP/CN-PMS* complex, resulting in a higher TOC removal efficiency of TCH compared to CN, with 21.1% of enhancement in removal efficiency. The surface-mediated electron transfer-dominated 3PVP/CN/PMS/vis system could selectively decompose highly hydrophilic contaminants and remove secondary effluent with 58.0% of COD, 88.1% of TP, 100.0% of NH_4^+-N and 67.8% of TN in a continuous flow reactor, which was of great environmental significance. This study introduced a novel approach to construct a surface-mediated electron transfer nonradical oxidation system, aiming to achieve stable and efficient decontamination of practical wastewater.

CRediT authorship contribution statement

Jingjing Jiang: Conceptualization, Visualization, Investigation, Data curation, Writing-original draft; **Chenli Yue**: Conceptualization, Visualization, Investigation, Data curation; **Ziqing Zhao**: Validation, Investigation; **Di Wu**: Validation, Investigation; **Shengda Liu**: Validation, Investigation; **Yanan Zhang**: Data curation, Formal analysis; **Bowen Zhao**: Data curation, Formal analysis; **Zhenhao Zhao**: Data curation, Formal analysis; **Yansong Liu**: Writing-review & editing; **Cong Lyu**: Writing-review & editing; **Chongjun Zhang**: Writing-review & editing; **Mingxin Huo**: Writing-review & editing; **Dandan Zhou**: Writing-review & editing; **Shuangshi Dong**: Resources, Supervision, Funding acquisition, Writing-review & editing, Project administration.

Declaration of Competing Interest

The authors declare that they have no known competing financial interests or personal relationships that could have appeared to influence the work reported in this paper.

Data Availability

Data will be made available on request.

Appendix A. Supporting information

Supplementary data associated with this article can be found in the online version at doi:10.1016/j.apcatb.2024.124153.

References

[1] H.L. Yang, R.L. Qiu, Y.T. Tang, S.J. Ye, S.H. Wu, F.Z. Qin, L. Xiang, X.F. Tan, G. M. Zeng, M. Yan, Carbonyl and defect of metal-free char trigger electron transfer and $O_2^{\bullet-}$ in persulfate activation for aniline aerofloat degradation, Water Res 231 (2023) 119659.

[2] J. Wang, X.G. Duan, J. Gao, Y. Shen, X.H. Feng, Z.J. Yu, X.Y. Tan, S.M. Liu, S. B. Wang, Roles of structure defect, oxygen groups and heteroatom doping on

carbon in nonradical oxidation of water contaminants, Water Res 185 (2020) 116244.

[3] J. Miao, W. Geng, J.J. Alvarez, M.C. Long, 2D N-doped porous carbon derived from polydopamine-coated graphitic carbon nitride for efficient nonradical activation of peroxymonosulfate, Environ. Sci. Technol. 54 (2020) 8473–8481.

[4] J.J. Jiang, Z.Q. Zhao, J.Y. Gao, T.R. Li, M.Y. Li, D.D. Zhou, S.S. Dong, Nitrogen vacancy-modulated peroxymonosulfate nonradical activation for organic contaminant removal via high-valent cobalt-oxo species, Environ. Sci. Technol. 56 (2022) 5611–5619.

[5] G.L. Zhou, S.Z. Wen, J.Y. Wang, X.L. Zhou, Y. Xu, Y. Guan, F.X. Zhu, J.Z. Yin, C. Liu, L.L. Zhang, Shorten migration distance of ROS and accelerate electron transfer by engineering dual Lewis acid sites for synergistic activation of PMS toward rapid TC degradation, Sep. Purif. Technol. 330 (2024) 125244.

[6] H.B. Ming, P.Y. Zhang, Y. Yang, Y. Zou, C. Yang, Y.D. Hou, K.N. Ding, J.S. Zhang, X.C. Wang, Tailored poly-heptazine units in carbon nitride for activating peroxymonosulfate to degrade organic contaminants with visible light, Appl. Catal. B: Environ. Energy 311 (2022) 121341.

[7] M.X. Yang, Z.X. Hou, X. Zhang, B.Y. Gao, Y.W. Li, Y.N. Shang, Q.Y. Yue, X.G. Duan, X. Xu, Unveiling the origins of selective oxidation in single-atom catalysis via Co−N₄−C intensified radical and nonradical pathways, Environ. Sci. Technol. (2022) 11635–11645.

[8] C. Yu, Z.Y. Zhao, Y. Zong, L.Q. Xu, B. Zhang, D.L. Wu, Electric field-enhanced coupled with metal-free peroxymonosulfate activator: the selective oxidation of nonradical species-dominated system, Water Res 227 (2022) 119323.

[9] F. Chen, L.L. Liu, J.J. Chen, W.W. Li, Y.P. Chen, Y.J. Zhang, J.H. Wu, S.C. Mei, Q. Yang, H.Q. Yu, Efficient decontamination of organic pollutants under high salinity conditions by a nonradical peroxymonosulfate activation system, Water Res. 191 (2021) 116799.

[10] Y.P. Wang, C. Liu, Y.T. Zhang, W.D. Meng, B. Yu, S.Y. Pu, D.H. Yuan, F. Qi, B.B. Xue, W. Chu, Sulfate radical-based photo-Fenton reaction derived by CuBi₂O₄ and its composites with α-Bi₂O₃ under visible light irradiation: catalyst fabrication, performance and reaction mechanism, Appl. Catal. B: Environ. Energy 235 (2018), 264–2.

[11] T.T. Lian, Y. Wang, B.L. Wu, F. Yang, N.V. Tarakina, M. Antonietti, 'Green-to-Green': Iron oxides embedded in lignin-based carbon scaffolds for water remediation via oxidation excluding free-radical pathways, J. Hazard. Mater. 442 (2023) 130070.

[12] G.L. Wang, Y.C. Liu, X.L. Dong, X.F. Zhang, Transforming radical to non-radical pathway in peroxymonosulfate activation on nitrogen doped carbon sphere for enhanced removal of organic pollutants: Combined effect of nitrogen species and carbon structure, J. Hazard. Mater. 437 (2022) 129357.

[13] I. Othman, J.H. Zain, M.A. Haija, F. Banat, Catalytic activation of peroxymonosulfate using CeVO₄ for phenol degradation: An insight into the reaction pathway, Appl. Catal. B: Environ. Energy 266 (2020) 11860.

[14] W. Ren, G. Nie, P. Zhou, H. Zhang, X.G. Duan, S.B. Wang, The intrinsic nature of persulfate activation and N-doping in carbocatalysis, Environ. Sci. Technol. 54 (2020) 6438–6447.

[15] J.J. Fu, Z. Mo, H.X. Chen, Z.G. Chen, X.L. Zhu, J. Yan, J.Y. Liu, Y.C. Wei, H.M. Li, H. Xu, Three coordinate nitrogen (N3c) vacancies from in-situ hydrogen bondbreaking over polymeric carbon nitride for efficient photocatalysis, J. Environ. Chem. Eng. 11 (2023) 109495.

[16] Y.Y. Kang, Y.Q. Yang, L.C. Yin, X.D. Kang, L.Z. Wang, G. Liu, H.M. Cheng, Selective breaking of hydrogen bonds of layered carbon nitride for visible light photocatalysis, Adv. Mater. 28 (2016) 6471–6477.

[17] Y.Y. Li, B.X. Zhou, H.W. Zhang, S.F. Ma, W.Q. Huang, W. Peng, W.Y. Hu, G.F. Huang, Doping-induced enhancement of crystallinity in polymeric carbon nitride nanosheets to improve their visible-light photocatalytic activity, Nanoscale 11 (2019) 6876–6885.

[18] W. Ren, G. Nie, P. Zhao, H. Zhang, X.G. Duan, S.B. Wang, The intrinsic nature of persulfate activation and N-doping in carbocatalysis, Environ. Sci. Technol. 54 (2020) 6438–6447.

[19] B. Anupama, T. Raguram, K.S. Rajni, Synthesis and characterization of cobalt nickel oxide (CoNi₂O₄) prepared by one step hydrothermal method, Mater. Today.: Proc. 64 (2022), 1694–17.

[20] H.Y. Li, N. Wang, H. Li, Z.Q. Ren, W.J. Ma, J. Li, Y.C. Du, Q. Xu, Polyvinylpyrrolidone-induced size-dependent catalytic behavior of Fe sites on N-doped carbon substrate and mechanism conversion in Fenton-like oxidation reaction, Appl. Catal. B: Environ. Energy 341 (2024) 123323.

[21] J.J. Jiang, S.D. Liu, D.L. Shi, T.Z. Sun, Y.K. Wang, S.Z. Fu, Y.S. Liu, M.Y. Li, D.D. Zhou, S.S. Dong, Spin state-dependent in-situ photo-Fenton-like transformation from oxygen molecule towards singlet oxygen for selective water decontamination, Water Res 244 (2023) 120502.

[22] G.G. Zhang, L.H. Lin, G.S. Li, Y.F. Zhang, A. Savateev, S. Zafeiratos, X.C. Wang, M. Antonietti, Ionothermal synthesis of triazine–heptazine-based copolymers with apparent quantum yields of 60% at 420nm for solar hydrogen production from"sea water", Angew. Chem. Int. Ed. 57 (2018) 9372–9376.

[23] W. Iqbal, B.C. Qiu, Q.H. Zhu, M.Y. Xing, J.L. Zhang, Self-modified breaking hydrogen bonds to highly crystalline graphiticcarbon nitrides nanosheets for drastically enhanced hydrogen production, Appl. Catal. B: Environ. 232 (2018) 306–313.

[24] N.N. Vu, S. Kaliaguine, T.O. Do, Selective fragmentation through C–N bond cleavage of carbon nitride framework for enhanced photocatalytic hydrogen production, ACS Sustain. Chem. Eng. 8 (2020) 853–863.

[25] Z.Q. Wang, G.X. Ding, J.T. Zhang, X.Q. Lv, P. Wang, S. Li, C.X. Li, Y.H. Ni, G.F. Liao, Critical role of hydrogen bonding between microcrystalline cellulose and g-C₃N₄ enables highly efficient photocatalysis, Chem. Commun. 60 (2024) 204–207.

[26] B. Li, Y. Si, B.X. Zhou, Q. Fang, Y.Y. Li, W.Q. Huang, W.Y. Hu, A.L. Pan, X.X. Fan, G.F. Huang, Doping-induced hydrogen-bond engineering in polymeric carbon nitride to significantly boost the photocatalytic H₂ evolution performance, ACS Appl. Mater. Interfaces 11 (2019) 17341–17349.

[27] H.C. Lan, L.L. Li, X.Q. An, F. Liu, C.B. Chen, H.J. Liu, J.H. Qu, Microstructure of carbon nitride affecting synergetic photocatalytic activity: Hydrogen bonds vs. structural defects, Appl. Catal. B: Environ. 204 (2017) 49–57.

[28] X.H. Guo, Y. Tian, M.C. Zhang, Y. Li, R. Wen, X. Li, X.F. Li, Y. Xue, L.J. Ma, C.Q. Xia, S.J. Li, Mechanistic insight into hydrogen-bond-controlled crystallinity and adsorption property of covalent organic frameworks from flexible building blocks, Chem. Mater. 30 (2018) 2299–2308.

[29] K.H. Lam, T.R. Bao, Z.E. Oi, J. Zhang, A.C. Grimsdale, Y.M. Lam, Enhancing the performance of solution-processed bulk-heterojunction solar cells using hydrogen-bonding-induced self-organization of small molecules, ACS Appl. Mater. Interfaces 5 (2013) 13265–13274.

[30] S. Li, Y.L. Yang, H.S. Zheng, Y.J. Zheng, C.S. He, B. Lai, J. Ma, J. Nan, Introduction of oxygen vacancy to manganese ferrite by Co substitution for enhanced peracetic acid activation and ¹O₂ dominated tetracycline hydrochloride degradation under microwave irradiation, Water Res 225 (2022) 119176.

[31] H.F. Xiong, S.S. Dong, J. Zhang, D.D. Zhou, B.E. Rittmann, Roles of an easily biodegradable co-substrate in enhancing tetracycline treatment in an intimately coupled photocatalyticbiological reactor, Water Res 136 (2018) 75–83.

[32] M. Zhang, J.Q. Ruan, X.H. Wang, W.Z. Shao, Z.L. Chen, Z.H. Chen, C. Gu, W.C. Qiao, J.S. Li, Selective oxidation of organic pollutants based on reactive oxygen species and the molecular structure: degradation behavior and mechanism analysis, Water Res 246 (2023) 120697.

[33] S.H. Zhou, J.W. Zhu, Z.R. Wang, Z. Yang, W.B. Yang, Z.L. Yin, Defective MOFs-based electrocatalytic self-cleaning membrane for wastewater reclamation: Enhanced antibiotics removal, membrane fouling control and mechanisms, Water Res 220 (2022) 118635.

[34] J.J. Fu, Z. Mo, H.X. Chen, Z.G. Chen, X.L. Zhu, J. Yan, J.Y. Liu, Y.C. Wei, H.M. Li, H. Xu, Three coordinate nitrogen (N3c) vacancies from in-situ hydrogen bondbreaking over polymeric carbon nitride for efficient photocatalysis, J. Environ. Chem. Eng. 11 (2023) 109495.

[35] S.N. Hua, D.C. Jiang, L. Gua, G.S. Xua, Z.J. Li, Y.P. Yuan, Awakening n→π* electronic transition by breaking hydrogen bonds in graphitic carbon nitride for increased photocatalytic hydrogen generation, Chem. Eng. J. 399 (2020) 1258.

[36] Y.L. He, C.S. He, L.D. Lai, P. Zhou, H. Zhang, L.L. Li, Z.K. Xiong, Y. Mu, Z.C. Pan, G. Yao, B. Lai, Activating peroxymonosulfate by N and O co-doped porous carbon for efficient BPA degradation: a re-visit to the removal mechanism and the effects of surface unpaired electrons, Appl. Catal. B: Environ. 314 (2022) 121390.

[37] X.N. Wang, J.P. Jia, Y.L. Wang, Combination of photocatalysis with hydrodynamic cavitation for degradation of tetracycline, Chem. Eng. J. 315 (2017) 274–282.

[38] C. Fang, S.H. Wang, H.B. Xu, Q. Huang, Degradation of tetracycline by atmospheric-pressure non-thermal plasma: Enhanced performance, degradation mechanism, and toxicity evaluation, Sci. Total Environ. 812 (2022) 152455.

[39] D.Y. Lin, P. Duan, W.T. Yang, X.J. Huang, Y.J. Zhao, C.T. Wang, Q.H. Pan, Facile fabrication of melamine sponge@covalent organic framework composite for enhanced degradation of tetracycline under visible light, Chem. Eng. J. 430 (2022) 132817.

[40] S.S. Xin, S.Y. Huo, C.L. Zhang, X.M. Ma, W.J. Liu, Y.J. Xin, M.C. Gao, Coupling nitrogen/oxygen self-doped biomass porous carbon cathode catalyst with CuFeO₂/biochar particle catalyst for the heterogeneous visible-light driven photo-electro-Fenton degradation of tetracycline, Appl. Catal. B: Environ. Energy 305 (2022) 121024.

[41] S.S. Xin, G.C. Liu, X.H. Ma, J.X. Gong, B.R. Ma, Q.H. Yan, Q.H. Chen, D. Ma, G.S. Zhang, M.C. Gao, Y.J. Xin, High efficiency heterogeneous Fenton-like catalyst biochar modified CuFeO₂ for the degradation of tetracycline: economical synthesis, catalytic performance and mechanism, Appl. Catal. B: Environ. Energy 280 (2021) 1193.

[42] L. Wang, X.P. Lu, G.D. Chen, Y.Z. Zhao, S.L. Wang, Synergy between MgFe₂O₄ and biochar derived from banana pseudo-stem promotes persulfate activation for efficient tetracycline degradation, Chem. Eng. J. 468 (2023) 143773.

[43] H. Zhang, Q. An, Y. Su, X. Quan, S. Chen, Co₃O₄ with upshifted d-band center and enlarged specific surface area by single-atom Zr doping for enhanced PMS activation, J. Hazard. Mater. 448 (2023) 130987.

[44] Z.X. Hou, X. Zhang, B.Y. Gao, Y.W. Li, Y.N. Shang, Q.Y. Yue, X.G. Duan, X. Xu, Unveiling the origins of selective oxidation in single-atom catalysis via Co−N₄−C intensified radical and nonradical pathways, Environ. Sci. Technol. 56 (2022) 11635–11645.

[45] Z.Y. Guo, Y. Si, W.Q. Xia, F. Wang, H.Q. Liu, C. Yang, W.J. Zhang, W.W. Li, Electron delocalization triggers nonradical Fenton-like catalysisover spinel oxides, PNAS 119 (31) (2022) e2201607119.

[46] P. Zhou, Y.Y. Yang, W. Ren, X.J. Li, Y.L. Zhang, B. Lai, S.B. Wang, X.G. Duan, Molecular and kinetic insights to boron boosted Fenton-like activation of peroxymonosulfate for water decontamination, Appl. Catal. B: Environ. Energy 319 (2022) 121916.

[47] Y. Wei, J. Miao, J.X. Ge, J.Y. Lang, C.Y. Yu, L.Z. Zhang, J.J. Alvarez, M.C. Long, Ultrahigh peroxymonosulfate utilization efficiency over CuO nanosheets via heterogeneous Cu(III) formation and preferential electron transfer during degradation of phenols, Environ. Sci. Technol. 56 (2022) 8984–8992.

[48] J. Liang, X.G. Duan, X.Y. Xu, K.X. Chen, Y. Zhang, L. Zhao, H. Qiu, S.B. Wang, X.D. Cao, Persulfate oxidation of sulfamethoxazole by magnetic iron-char composites via nonradical pathways: Fe(IV) versus surface mediated electron transfer, Environ. Sci. Technol. 55 (2021) 10077–10086.